

The ultraviolet photodissociation of Cl₂O at 235 nm and of HOCl at 235 and 266 nm

Yoshiki Tanaka, Masahiro Kawasaki, Yutaka Matsumi, Hisashi Fujiwara, Takashi Ishiwata, Leon J. Rogers, Richard N. Dixon, and Michael N. R. Ashfold

Citation: *The Journal of Chemical Physics* **109**, 1315 (1998); doi: 10.1063/1.476682

View online: <http://dx.doi.org/10.1063/1.476682>

View Table of Contents: <http://scitation.aip.org/content/aip/journal/jcp/109/4?ver=pdfcov>

Published by the [AIP Publishing](#)

Articles you may be interested in

[Cl₂O photochemistry: Ultraviolet/vis absorption spectrum temperature dependence and O\(3P\) quantum yield at 193 and 248 nm](#)

J. Chem. Phys. **134**, 204310 (2011); 10.1063/1.3592662

[C–Cl bond fission dynamics and angular momentum recoupling in the 235 nm photodissociation of allyl chloride](#)

J. Chem. Phys. **121**, 11016 (2004); 10.1063/1.1812757

[On the ultraviolet photodissociation of H₂Te](#)

J. Chem. Phys. **121**, 9389 (2004); 10.1063/1.1799572

[Photodissociation of CSCI₂ at 235 nm: Kinetic energy distributions and branching ratios of Cl atoms and CSCI radicals](#)

J. Chem. Phys. **117**, 1123 (2002); 10.1063/1.1480272

[The ultraviolet photodissociation dynamics of hydrogen bromide](#)

J. Chem. Phys. **110**, 281 (1999); 10.1063/1.478063



The ultraviolet photodissociation of Cl₂O at 235 nm and of HOCl at 235 and 266 nm

Yoshiki Tanaka^{a)} and Masahiro Kawasaki

Department of Molecular Engineering, Kyoto University, Kyoto 606-01, Japan

Yutaka Matsumi

Solar Terrestrial Environmental Laboratory, Nagoya University, Toyokawa 442, Japan

Hisashi Fujiwara and Takashi Ishiwata

Faculty of Information Science, Hiroshima City University, Hiroshima 731-31, Japan

Leon J. Rogers, Richard N. Dixon, and Michael N. R. Ashfold

School of Chemistry, University of Bristol, Bristol BS8 1TS, United Kingdom

(Received 19 February 1998; accepted 16 April 1998)

The primary photochemistry of gas phase dichlorine monoxide (Cl₂O) and of hypochlorous acid (HOCl) following excitation at 235 nm has been investigated using photofragment ion imaging to obtain the recoil velocity and angular distributions of the ground (²P_{3/2}) and spin-orbit excited (²P_{1/2}) atomic chlorine products. In the case of Cl₂O, both Cl spin-orbit products exhibit angular distributions characterized by an anisotropy parameter, $\beta = 1.2 \pm 0.2$, consistent with previous interpretations of the ultraviolet (UV) absorption spectrum of Cl₂O which associate the broad intense absorption feature peaking at $\lambda \sim 255$ nm with excitation to a (bent) dissociative state of ¹B₂(C_{2v}) symmetry. The recoil velocity distributions of the two Cl spin-orbit products are markedly different. The ground state atoms (which constitute >90% of the total Cl atom yield) are partnered by ClO fragments carrying significantly higher average levels of internal excitation. The slowest Cl atoms are most readily understood in terms of three body fragmentation of Cl₂O to its constituent atoms. These findings are rationalized in terms of a model potential energy surface for the ¹B₂ state, which correlates diabatically with ClO(X) radicals together with a spin-orbit excited Cl atom, with efficient radiationless transfer to one (or more) lower energy surfaces at extended Cl-O bond lengths accounting for the dominance of ground state Cl atom fragments. The image of the ground state Cl atoms resulting from photolysis of HOCl at 235 nm is consistent with parent excitation via a transition for which the dipole moment is closely aligned with the Cl-O bond, followed by prompt dissociation ($\beta = 1.7 \pm 0.2$) with the bulk of the excess energy partitioned into product recoil. Such conclusions are consistent with the results of laser induced fluorescence measurements of the OH(X) products resulting from 266 nm photodissociation of HOCl which reveal OH(X) products in both spin-orbit states, exclusively in their zero-point vibrational level, and carrying only modest levels of rotational excitation (well described by a Boltzmann distribution with $T_{\text{rot}} \sim 750 \pm 50$ K).

© 1998 American Institute of Physics. [S0021-9606(98)01328-2]

INTRODUCTION

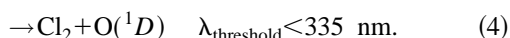
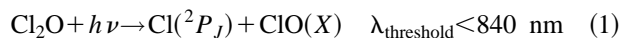
Cl atoms, ClO and OH radicals, through the ClO_x and HO_x cycles, all play a role in the catalyzed destruction of global stratospheric ozone.^{1,2} Though dichlorine monoxide, Cl₂O, is currently thought to play at most a minor role in stratospheric chemistry, its hydrate, hypochlorous acid (HOCl), is an important chlorine reservoir species.³ Consequently, the near UV spectroscopy and photochemistry of HOCl has received considerable attention, both experimental⁴⁻⁹ and theoretical,¹⁰⁻¹⁴ since its photochemical stability directly affects its atmospheric lifetime and thus its importance in atmospheric chemistry. HOCl exhibits a broad diffuse absorption at wavelengths $\lambda < 360$ nm, with a maximum at ~ 250 nm ($\sigma \sim 4 \times 10^{-19}$ cm² molecule⁻¹) and a

“shoulder” at $\lambda \sim 300$ nm.^{4,5,15} Comparison with *ab initio* theory^{10,12} suggests that the dominant absorption at these wavelengths is associated with the ²1A' - \tilde{X} 1A' transition, but that the ¹1A'' - \tilde{X} 1A' perpendicular transition will contribute some oscillator strength at the longer excitation wavelengths. Experimental measurements of the alignment of the OH(X) fragments arising in the 248⁷ and 266 nm⁸ photolysis of HOCl both indicate that these fragments arise following prompt dissociation of an excited state of ¹A' symmetry, though time-of-flight (TOF) measurements of the partner Cl atoms formed in HOCl photodissociation at wavelengths ~ 235 nm gave somewhat less conclusive results.⁹

The spectroscopy and photochemistry of Cl₂O have received rather less attention. It has a bent (C_{2v}) ground state geometry, with $r_0(\text{Cl-O}) = 1.696$ Å and $\angle \text{ClOCl} = 110.9^\circ$.^{16,17} Cl₂O exhibits a continuous absorption spectrum, with maxima at $\sim 530, 420, 255$ and 170 nm, beyond

^{a)}On leave from Graduate School of Environmental Science, Hokkaido University, Sapporo 060, Japan.

which comes the first Rydberg origin, at 162.9 nm.^{4,15,18–22} Cl₂O photolysis finds use as a convenient source of ClO radicals and Cl atoms in laboratory experiments relevant to atmospheric chemistry, but detailed, quantum state resolved studies of its primary photochemistry and the accompanying photodissociation dynamics remain rare. Early studies of Cl₂O photolysis,^{23–27} reviewed elsewhere,^{21,28} showed reaction (1) to be the dominant fragmentation pathway at all near UV excitation wavelengths but also suggested that one or more of channels (2)–(4) must be responsible for the minor O atom yield identified when photolyzing at the shorter UV wavelengths,



Note that the long wavelength limits quoted correspond to thermodynamic thresholds,^{29–31} and make no allowance for any possible energy barriers in these various dissociation channels. More recently, Okumura, Minton and co-workers^{28,32} have studied the photolysis of jet-cooled Cl₂O molecules at three excimer laser wavelengths (193, 248 and 308 nm), using traditional photofragment translational spectroscopy techniques with mass spectrometric detection of products with m/z 16 (O⁺), 35 (Cl⁺), 51 (ClO⁺) and 70 (Cl₂⁺). They confirm Cl-O bond fission [channel (1)] as the sole primary fragmentation pathway following excitation at 308 nm. 248 nm photolysis results in ClO fragments with a broad, apparently bimodal, spread of internal energies, and some three body dissociation. This latter atomization process (2) is found to be dominant when Cl₂O is photolyzed at 193 nm; the authors²⁸ suggest that these products arise via the concerted eliminations (3) and (4) and subsequent fragmentation of the highly vibrationally excited Cl₂ products.

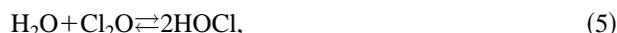
Here we report state-specific and angle and velocity resolved measurements of the Cl atomic products resulting from photolysis of jet-cooled HOCl and Cl₂O molecules at wavelengths around 235 nm using the technique of photofragment ion imaging, first introduced by Chandler and Houston.^{33,34} The technique provides a direct two-dimensional (2D) visualization of the laboratory-frame photofragment velocity distributions and, as such, provides a particularly powerful route to elucidating the full 3D center-of-mass frame photofragment velocity distributions.

EXPERIMENT

A single excimer pumped dye laser, the output of which was frequency doubled in BBO, was used to generate the necessary radiation at wavelengths ~ 235 nm required both for photodissociating the Cl₂O and HOCl precursors and to effect the two-photon resonance enhanced multiphoton ionization (REMPI) of the Cl atom photofragments. As previously,^{35–37} ground Cl(²P_{3/2}) and spin-orbit excited Cl*(²P_{1/2}) atomic photoproducts were probed using wavelengths of 235.336 and 235.205 nm, respectively. Cl/Cl* branching ratios were estimated by adopting the relative ion-

ization probability $f(\text{Cl})/f(\text{Cl}^*) = 0.85 \pm 0.1$ as reported by Liyanage *et al.*³⁸ A few similar one color experiments searching for O(³P₂) atom products from Cl₂O photolysis were performed also; the requisite wavelength in this case was 225.65 nm, appropriate for 2 + 1 REMPI involving the O(2p³3p¹; ³P₂ ← 2p⁴; ³P₂) transition.³⁹

Cl₂O was prepared by the method of Cady,⁴⁰ in which a low pressure of Cl₂ gas (<50 Torr) was flowed slowly over dried HgO dispersed on glass beads held at room temperature. The effluent gas was collected in a trap maintained at liquid N₂ temperature. Residual Cl₂ in the condensed product was removed by vacuum distillation at -112 °C. The purity of the final Cl₂O sample was verified by UV absorption spectroscopy.¹⁵ HOCl was prepared by mixing Cl₂O (5 Torr) with H₂O (13 Torr) and leaving to equilibrate. Given a value 0.082 ± 0.010 for the equilibrium constant K_5 ,^{31,41}



we estimate that the HOCl partial pressure in this mixture is ~ 1.5 Torr. Both the Cl₂O sample and the HOCl (as the HOCl/Cl₂O/H₂O equilibrium mixture) were seeded in Ar or Kr (typical mixing ratio $\sim 2\%$) and introduced into the ion imaging spectrometer in the form of a pulsed molecular beam with the backing pressure held at ~ 600 Torr. The measured images were insensitive to carrier gas, encouraging us to conclude that there is negligible clustering in the molecular beam. It was noticed that the signal level would deteriorate with time—an effect attributable to surface catalyzed decomposition in the delivery line leading to the pulsed valve. To counteract this, a flow system was used to ensure that the sample mixture immediately behind the valve was continually being refreshed.

Two different ion imaging apparatus, one in Kyoto, the other in Bristol, were used in the present experiments. The Kyoto apparatus, which follows the original design of Chandler and Houston,³³ has been described in detail elsewhere.⁴² Essential details of the Bristol apparatus have also been reported previously.^{37,43} It incorporates one innovative feature designed to improve the image fidelity—namely, the use of software to establish, on a shot by shot basis, which of the individual ion events in the image evident on the phosphor screen mounted behind the microchannel plates (MCPs) mounted at the end of the TOF tube satisfy user selected thresholds for minimum size and intensity, and to determine their centroids. The final image is built up by accumulating these centroids, while the laser frequency is scanned repeatedly across the Doppler profile of the relevant Cl/Cl* transition. As in all ion imaging experiments, the three-dimensional (3D) fragment velocity distribution is detected as a two-dimensional (2D) projection. Given the assumption of axial symmetry around the direction of the electric vector of the dissociation laser radiation, we employ a filtered back-projection method^{42,44} to extract the required 3D velocity distribution from the observed 2D images. The velocity (radial) scale of the resulting images was calibrated by imaging the Cl fragments arising in the well-documented 235.336 nm photolysis of ICl.³⁷ Figure 1(d) shows the equatorial slice through the reconstructed 3D image of these Cl atom frag-

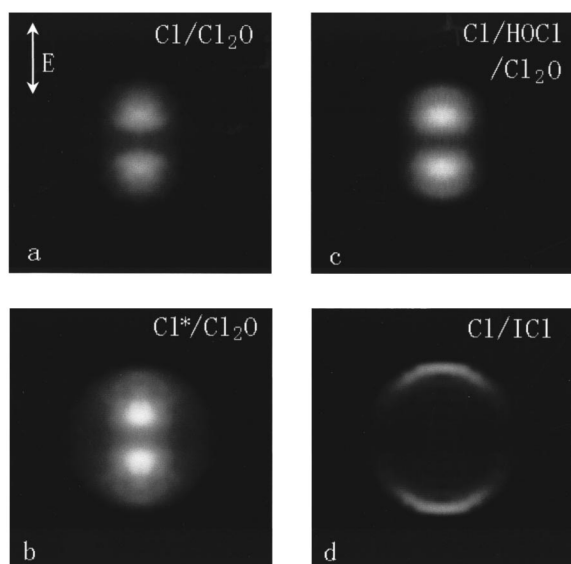


FIG. 1. Cl^+ ion images, displayed as equatorial slices through the reconstructed 3D distributions, from the photodissociation of Cl_2O (a) and (b), HOCl (c) and ICl (d) at 235 nm. The detected species (Cl or Cl^*) is indicated on each image. In each case the E vector of the photolysis laser radiation is aligned vertically, as shown by the arrow. Note that because of the limited available grey scale it has proved convenient to display the strongest image (a) with deceptively faint intensity, and that the Cl^+ signal in Fig. 1(c) contains contributions from Cl atoms arising from photolysis of both Cl_2O and HOCl.

ments; the width of this image ($\sim 60 \text{ kJ mol}^{-1}$ [full width at half maximum (FWHM)] at a Cl fragment translational energy $E_T = 213 \text{ kJ mol}^{-1}$) gives a measure of the prevailing instrumental resolution. Note that the image radius actually scales linearly with velocity, so the energy resolution should be E_T dependent. Thus, for example, for Cl fragments with $E_T = 100 \text{ kJ mol}^{-1}$ (closer to the mean Cl atom kinetic energy arising in the 235 nm photolysis of Cl_2O and HOCl), the FWHM energy resolution will be $\sim 40 \text{ kJ mol}^{-1}$. For consistency, all of the images shown in this work were recorded in Kyoto, but equivalent results for Cl_2O were obtained in Bristol also.

OH(X) photofragments resulting from the linearly polarized 266 nm photodissociation of HOCl (in a slowly flowing HOCl/ Cl_2O / H_2O equilibrated mixture, at room temperature and a total pressure of 0.1–0.2 Torr) were detected by laser induced fluorescence (LIF) on the $A-X$ (0,0) band at 308 nm using apparatus in Hiroshima. Full details of the experimental procedure and methods of data analysis are reported elsewhere.⁴⁵

RESULTS

Photodissociation of Cl_2O at 235 nm

Cl and Cl^* atomic fragments produced from Cl_2O photolysis at wavelengths $\sim 235 \text{ nm}$ were detected by 2+1 REMPI. The measured Cl signal intensity (at 235.336 nm) was about 15 times that for the Cl^* peak (measured at 235.205 nm) for the same incident laser pulse energy which, when allowing for the different ionization detection efficiencies for the two spin-orbit states,³⁸ leads to a $[\text{Cl}]/[\text{Cl}^*]$

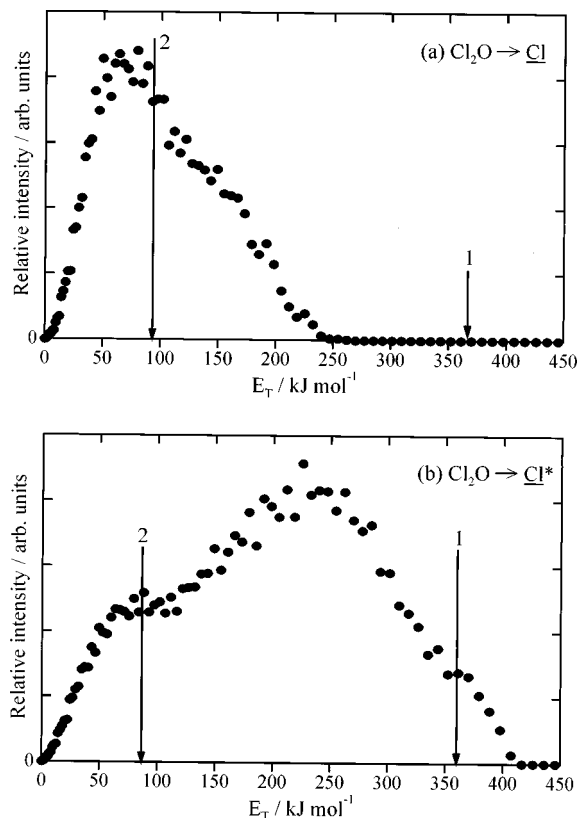


FIG. 2. Center-of-mass translational energy distribution, $P(E_T)$, of (a) the ground state $\text{Cl}(^2P_{3/2})$ products and (b) the spin-orbit excited $\text{Cl}^*(^2P_{1/2})$ products arising in the 235 nm photodissociation of Cl_2O . The maximum fragment kinetic energies allowed by energy conservation following dissociation via channels (1) and (2) are indicated.

branching ratio of 13 ± 2 . The Cl and Cl^* photofragment images shown in Figs. 1(a) and 1(b) are the equatorial slices through the 3D velocity distributions that have been extracted from the raw 2D projections, after symmetrizing, using the filtered back-projection method. The Cl and Cl^* images show essentially identical angular distributions relative to the direction of the E vector of the photolysis laser radiation, but careful inspection shows their relative sizes (i.e., the Cl and Cl^* recoil velocity distributions) to be different; the ground state Cl atoms are formed with less average kinetic energy.

Center-of-mass (CM) translational energy distributions, $P(E_T)$, for the Cl and Cl^* atom products are shown in Fig. 2. Also marked on these plots are the maximum possible kinetic energy releases for chlorine atoms arising via channels (1) and (2) given the photon energy and the respective bond dissociation energies $D_0(\text{Cl-OCl}) = 141^{29,30}$ and $D_0(\text{Cl-O}) = 265 \text{ kJ mol}^{-1}$.⁴⁶ In constructing these, we assume the counter fragment to have a mass appropriate for ClO. We recognize the inaccuracy of such a procedure for all Cl fragments that arise via the three body fragmentation process (2) and thus caution against reading too much into the detailed form of the lowest energy part of these $P(E_T)$ distributions. Clearly, however, and notwithstanding the limited energy resolution of the experiment, the ClO fragments partnering the ground state Cl atoms are formed with significant (and a broad spread of) internal excitation. The Cl^* atom

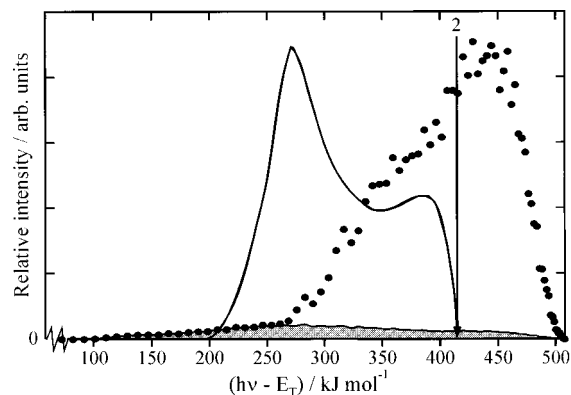


FIG. 3. Comparison of product translational energy distributions resulting from Cl_2O photolysis at 248 nm (solid line, obtained by monitoring ions with m/z 51, after Ref. 28) and at 235 nm (by imaging the Cl atom products). The shaded area represents the Cl^* yield, while the filled points indicate the total Cl atom yield obtained by summing the deduced $P(E_T)$ distributions for Cl and Cl^* atoms, weighted in the ratio 13:1. For the purposes of this comparison the horizontal scale is $(h\nu - E_T)$. Note that much of the present signal appearing at energies in excess of $D_0(\text{Cl}-\text{O})$ —indicated by the vertical arrow—is attributed to the three body dissociation (2); any corresponding products arising in the 248 nm photolysis of Cl_2O will not appear in the solid line distribution because of the detection method used (Refs. 28 and 32).

products exhibit an even broader E_T distribution [Fig. 2(b)] but, relative to the Cl products, the center of gravity of the Cl^* distribution falls at much higher translational energies (i.e., lower ClO internal energies).

Okumura, Minton and co-workers^{28,32} have reported $P(E_T)$ spectra, obtained by conventional TOF methods followed by electron bombardment and mass spectrometric detection, for the Cl+ClO products resulting from 248 nm photolysis of Cl_2O . These they have chosen to fit, arbitrarily, in terms of three Gaussian distributions centered at $\langle E_T \rangle = 74$, 150 and 214 kJ mol^{-1} , respectively. Such mass spectrometric measurements are, of necessity, non-spin-orbit state selective, though we note that Chichinin⁴⁷ has reported that $18\% \pm 2\%$ of the total Cl atom yield arising in the 248 nm photolysis of Cl_2O is in the spin-orbit excited Cl^* state. Clearly, we can compare this earlier $P(E_T)$ data with an appropriately weighted sum of the distributions shown in Figs. 2(a) and 2(b). Figure 3 shows such a comparison, where we have chosen to use as the horizontal scale $(h\nu - E_T)$, i.e., to offset the experimentally derived $P(E_T)$ distributions by an amount equal to the difference in the 235 and 248 nm photon energies and then align the spectra in terms of the ClO internal energy. The distribution obtained at 248 nm shows some similarities with the present data (after summing over both spin-orbit states), despite the difference in photolysis wavelength; in both cases the distribution appears bimodal and the ClO fragments are deduced to be formed in a wide spread of internal energy states, with little probability of being formed internally “cold.” We note the seemingly very different relative importance of the “slow” component in the two distributions but this is, in part, an artefact since the 248 nm distribution was generated by transforming TOF data recorded on the m/z 51 (ClO^+) mass channel only, and thus includes no contribution from slow

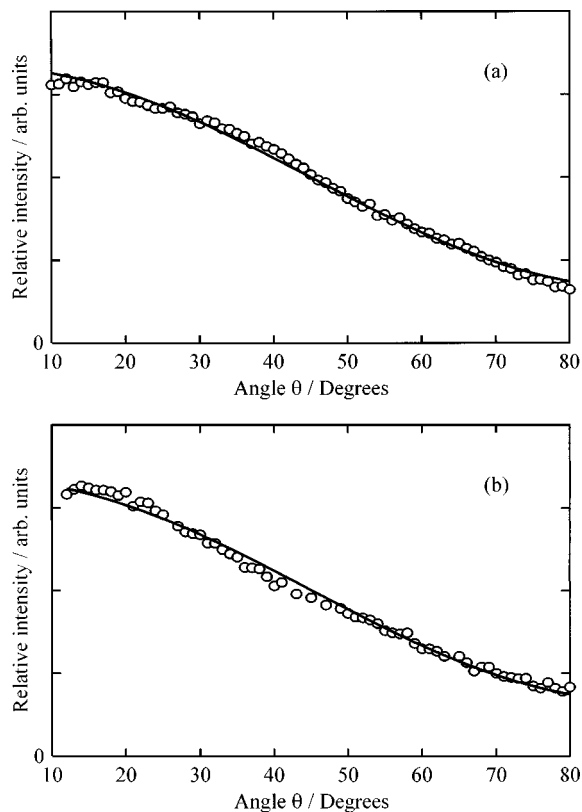


FIG. 4. Angular distributions of (a) Cl and (b) Cl^* atom yield (integrated over all recoil velocities) resulting from 235 nm photolysis of Cl_2O . The solid lines are best-fits to the data in terms of Eq. (6) with $\beta = 1.2$ and $\beta = 1.1$, respectively.

products arising via channel (2). We return to further discussion of these points, and of the likely nature of the ClO internal excitation, below.

Figure 4 shows plots of the angular distributions of the Cl and Cl^* products arising in the 235 nm photolysis of Cl_2O . The angular distribution of the photofragment velocity vector v is given by⁴⁸

$$I(v, \theta) = f(v) \cdot \{1 + \beta P_2(\cos \theta)\} / 4\pi, \quad (6)$$

where $f(v)$ is the speed distribution of the fragment, θ is the angle between the polarization vector of the photolysis laser radiation and the fragment recoil velocity vector, β is the anisotropy parameter and $P_2(\cos \theta)$ is the second order Legendre polynomial. From Fig. 4 we obtain best-fit values $\beta = 1.2 \pm 0.1$ for both the total Cl and the total Cl^* product flux distributions, with no discernible dependence upon v . Such a finding contradicts the results of the earlier 248 nm photolysis study by Moore *et al.*,³² who deduced the following best-fit β parameters for the three assumed subgroups within their $P(E_T)$ distribution: fast, $\beta = 0.7 \pm 0.2$; intermediate, $\beta = 1.5 \pm 0.2$; and slow, $\beta = 1.2 \pm 0.2$. We do not believe that this apparent discrepancy can be attributed to the low energy resolution of the present imaging apparatus since we can easily distinguish between overlapping Cl angular distributions with $\beta = 1.2$ and 1.7 (from 235 nm photolysis of Cl_2O and HOCl, respectively)—see below. The 225.65 nm photolysis of Cl_2O was also studied briefly since this is a suitable wavelength for inducing 2+1 REMPI of any $\text{O}(^3P_2)$ pho-

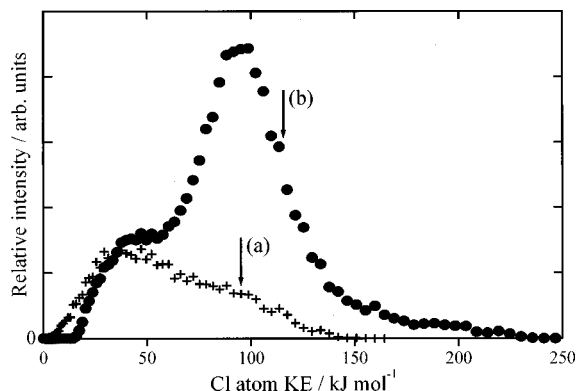
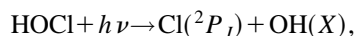


FIG. 5. Kinetic energy distribution [solid points, labeled (b)] of the ground state Cl atoms resulting from 235 nm photolysis of an HOCl/Cl₂O/H₂O mixture derived from the image shown in Fig. 1(c). The crosses show the corresponding Cl atom kinetic energy distribution obtained using a pure Cl₂O sample [labeled (a)], arbitrarily scaled (vertically) so as to account for most of the signal at KE~45 kJ mol⁻¹.

tofragments that may result. Signal levels were low, in part because of the weakness of the parent absorption at this wavelength. The resulting O atom image was small (indicating little translational energy release) and, notwithstanding the poor signal to noise ratios, showed little obvious anisotropy.

Photodissociation of HOCl at 235 nm

As shown in Fig. 1(c), an additional higher velocity, parallel component is evident in the ground state Cl atom image observed from the 235 nm photolysis of the equilibrium mixture of HOCl, Cl₂O and H₂O. This we associate with Cl atoms resulting from HOCl photolysis,



$$\lambda_{\text{threshold}} < 518 \text{ nm (Ref. 49),} \quad (7)$$

while the inner component is attributable to photolysis of Cl₂O. Since the Cl atoms from these two different precursors have different counter fragments we choose to plot the distribution of Cl atom kinetic energies [not the center-of-mass $P(E_T)$ distribution] in Fig. 5. The previously established kinetic energy distribution of the ground state Cl atoms resulting from 235 nm photolysis of Cl₂O [Fig. 2(a)] is replotted on the appropriate energy scale [crosses, curve marked (a)]; its vertical scaling has been chosen arbitrarily so as to account for most of the shoulder apparent at KE~45 kJ mol⁻¹. The profile mapped out by the data points labeled (b) is taken to be the translational energy distribution of the ground state Cl atoms resulting from 235 nm photolysis of HOCl, with an underlying contribution from the inevitable Cl₂O impurity. It peaks at 90 ± 10 kJ mol⁻¹, with an energy width of ~40 kJ mol⁻¹ (FWHM). As mentioned previously, an energy spread of this magnitude is largely attributable to the limited resolution of the ion imaging experiment. The corresponding center-of-mass translational energy of the OH+Cl fragments (280 ± 40 kJ mol⁻¹) accounts for all of the photon energy over and above that required to break the Cl—O bond, implying little internal excitation in the partner OH(X)

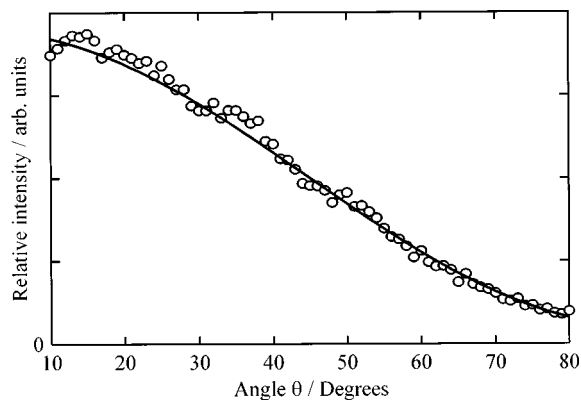


FIG. 6. Angular distribution of that fraction of the Cl atom product yield with KE>75 kJ mol⁻¹ resulting from 235 nm photolysis of the HOCl/Cl₂O/H₂O mixture (open circles). The solid line shows a best-fit to the experimental data in terms of Eq. (6) with $\beta=1.7$.

fragment as found experimentally in the case of HOCl photolysis at 248⁷ and 266 nm⁸ (and see below), and predicted theoretically.¹⁴

The angular distribution of the Cl fragments resulting from 235 nm photolysis of HOCl, shown in Fig. 6, is well described by an anisotropy parameter $\beta=1.7 \pm 0.2$, significantly higher than for the Cl atoms from Cl₂O photolysis at this wavelength. Note that, even though this plot shows the angular dependence of just the faster part of the entire Cl atom signal (KE>75 kJ mol⁻¹), this value is surely a lower limit given the presumed contribution of some Cl signal from the photolysis of Cl₂O (see Fig. 5). This high value is consistent with theoretical expectations^{10,12} that the $2^1A' - \tilde{X}^1A'$ parallel transition is the dominant contributor to the near UV absorption of HOCl at these wavelengths, and accords with the suggestions of Bell *et al.*,⁹ who observed the Doppler profile of Cl atoms formed in the 235 nm photolysis of HOCl and concluded that the dissociation process must be occurring on the steeply repulsive $2^1A'$ potential energy surface, resulting in fast Cl atoms with a relatively narrow kinetic energy distribution.

Photodissociation of HOCl at 266 nm

In parallel experiments, described more fully elsewhere,⁴⁵ the internal state population distribution within the OH($X^2\Pi$) fragments resulting from 266 nm photolysis of HOCl (in the HOCl/Cl₂O/H₂O equilibrium mixture), and their recoil velocity distributions, were investigated via measurement and analysis of the OH(A—X) LIF excitation spectrum at ~308 nm. Only OH($X_{v=0}$) fragments are detected; no indication of any vibrationally excited OH(X) products could be found. Figure 7 shows the OH($X_{v=0}$) rotational state population distributions, plotted in the form of Boltzmann plots, for each spin-orbit state ($\Omega=3/2$ and $1/2$). The individual data points were obtained by measuring the intensities of unblended P_i or R_i lines ($i=1, 2$ for the $\Omega=3/2$ and $1/2$ components, respectively), correcting for any variations in the photolysis and/or probe laser intensities, and dividing by the appropriate rotational line strength as listed by Dieke and Crosley.⁵⁰ As found previously,^{7,8} the OH($X_{v=0}$) rota-

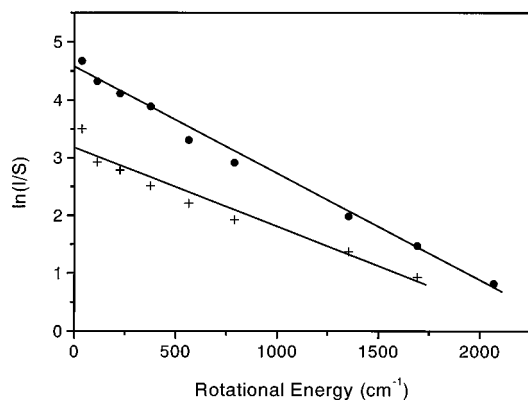


FIG. 7. Semilogarithmic plot of rotational state populations versus rotational energy for the OH(X , $\Omega = 1/2(+)$ and $3/2(\bullet)$, $v = 0$) fragments resulting from HOCl photodissociation at 266 nm. The solid lines show best fits to the data, and correspond to Boltzmann temperatures of 800 ($\Omega = 3/2$) and 770 K ($\Omega = 1/2$).

tional state population distributions are well represented by Boltzmann distributions with “temperatures” of 800 ± 70 K (for the $\Omega = 3/2$ component) and 770 ± 50 K ($\Omega = 1/2$), with the two spin-orbit components populated in the ratio $\Omega = 3/2/\Omega = 1/2 \sim 2:1$. Clearly, as at 235 nm, the OH(X) fragments resulting from 266 nm photolysis of HOCl are internally “cold,” with $\langle E_{\text{INT}} \rangle \sim 550 \text{ cm}^{-1}$ only. Analysis of the Doppler profiles of, for example, the $P_1(5)$ and $Q_1(4)$ transitions within the OH($A-X$) (0,0) band indicate that the OH fragments resulting from the 266 nm photodissociation of HOCl are formed with high recoil velocity (4100 m s^{-1}) and an angular anisotropy well described by $\beta = 1.3 \pm 0.1^{45}$ —broadly paralleling observations at 235 nm and suggesting that the $2^1A' - \tilde{X}^1A'$ transition still dominates the parent absorption at 266 nm.

DISCUSSION

Photodissociation of Cl₂O at 235 nm

The key observations requiring explanation are the angular anisotropy of the recoiling Cl fragments, the nature of the energy disposal amongst the fragments, and the sensitivity of this energy disposal to the spin-orbit state of the Cl atom. Nickolaisen *et al.*²¹ have calculated vertical excitation energies and oscillator strengths from the \tilde{X}^1A_1 ground state (and the lowest energy 1^3B_1 excited state) of Cl₂O to a number of excited singlet and triplet states and, as a result,

assigned the absorption maxima evident at ~ 255 and ~ 170 nm in terms of transitions from the \tilde{X}^1A_1 ground state to the 1^1B_2 state and the 2^1B_1 state, respectively; the shoulder on the long wavelength side of the intense 255 nm peak is most likely due to the $1^1B_1 \leftarrow \tilde{X}^1A_1$ transition. Table I lists relevant configurations and the resulting states that can derive therefrom in the limit of linear ($D_{\infty h}$) and bent (C_{2v}) geometries. All of the calculated transitions can be understood in terms of electron promotion from one of the higher occupied nonbonding or weakly bonding orbitals in the ground state configuration to orbitals that are antibonding with respect to Cl—O stretching. The present experimental findings support the theoretical predictions. The transition moment associated with a $1^1B_2 \leftarrow 1^1A_1$ is y -polarized in the molecular frame, i.e., parallel to a line connecting the two Cl atoms. If the equilibrium bond angle in the 1^1B_2 excited state is the same as in the ground state (110.9°), then the limiting β value in the case of an instantaneous dissociation would be given by $\beta = 2P_2(\cos \chi)$, where $\chi = (180 - 110.9)^\circ/2$ is the angle between μ and the recoil velocity vector, v . This yields a value $\beta = 1.0$, somewhat smaller than that observed experimentally for both the Cl and Cl* product forming channels. Thus we conclude that Cl₂O photolysis at 235 nm does indeed proceed via a $1^1B_2 \leftarrow 1^1A_1$ excitation followed by prompt fragmentation on a potential energy surface (or surfaces), the topology of which tends to encourage some small opening of the $\angle \text{ClOCl}$ bond angle (reducing χ from 34.5 to $\sim 31^\circ$ would result in $\beta = 1.2$).

From Figs. 2 and 3 we see that less than half of the excess energy [$h\nu - D_0(\text{Cl—OCl})$] is released into product translational energy. The lowest excited state of ClO observed experimentally, the $A^2\Pi$ state ($T_e = 31749.6 \text{ cm}^{-1}$),⁴⁶ lies too high in energy to be formed as a primary product in the 235 nm photolysis of ground state Cl₂O molecules. This is the only excited state of ClO that can arise from the $\pi^* \leftarrow \pi$ electron promotion, but Langhoff⁵¹ has predicted the presence of a weakly bound $4^2\Sigma^-$ state of ClO with $T_e \sim 18\,000 \text{ cm}^{-1}$, arising from a $\sigma^* \leftarrow \pi^*$ electron promotion. The present $P(E_T)$ spectra [Figs. 2(a) and 2(b)] show no obvious indication for any involvement of such a ClO product state and, henceforth, electronic excitation of the ClO fragment (other than the ground state spin-orbit splitting) is not considered further as a possible sink for that fraction of the excess energy not appearing in the form of product translation.

Dissociation from a bent geometry will induce a large

TABLE I. Configurations and resulting terms relevant for discussion of the valence states of Cl₂O in the limit of linear ($D_{\infty h}$) and bent (C_{2v}) geometries. The final column provides a complete listing of all spin-orbit components in C_{2v} symmetry relevant for constructing the correlation diagram shown in Fig. 9. Singlet components are shown in bold, while the superscripts are appropriate to the case of reduced (C_s) symmetry.

Configuration	Configuration	Configuration	Configuration	Configuration
$(D_{\infty h})$	Terms ($D_{\infty h}$)	(C_{2v})	Terms (C_{2v})	Components (C_{2v})
$\dots \pi_g^4 \pi_u^4$	$1^1\Sigma_g^+$	$\dots a_1^2 b_2^2 a_2^2 b_1^2$	1^1A_1	\mathbf{a}'_1
$\dots \pi_g^4 \pi_u^3 \sigma_g^1$	$1^1\Pi_u; 3^3\Pi_u$	$\dots a_1^2 b_2^2 a_2^2 b_1^1 a_1^1$	$1^1B_1; 3^3B_1$	$a'_1, a'_2, \mathbf{b}'_1, b'_2$
$\dots \pi_g^3 \pi_u^4 \sigma_g^1$	$1^1\Pi_g; 3^3\Pi_g$	$\dots a_1^1 b_2^2 a_2^2 b_1^2 a_1^1$	$1^1A_1; 3^3A_1$	$\mathbf{a}'_1, a'_2, \mathbf{b}'_1, b'_2$
		$\dots a_1^2 b_2^2 a_2^1 b_1^2 a_1^1$	$1^1A_2; 3^3A_2$	$a'_1, \mathbf{a}'_2, \mathbf{b}'_1, b'_2$
		$\dots a_1^2 b_2^1 a_2^2 b_1^2 a_1^1$	$1^1B_2; 3^3B_2$	$a'_1, a'_2, \mathbf{b}'_1, \mathbf{b}'_2$

torque on the ClO fragment; a simple impact parameter model based on the ground state geometry and assuming $\langle E_T \rangle = 150 \text{ kJ mol}^{-1}$ would predict that the most populated state of the ClO partner would have rotational quantum number $N_{m.p.} \sim 80$ and a mean rotational energy $\langle E_{ROT} \rangle \sim 4000 \text{ cm}^{-1}$ (48 kJ mol^{-1}). This is sufficient to account for some, but by no means all, of the observed spread of internal energies in the ClO fragment. Neither does it provide any obvious explanation for the complete absence of fast ($E_T > 250 \text{ kJ mol}^{-1}$) products in the channel leading to ground state Cl atoms. However, the realization that the ClO(*X*) fragments are likely to be formed with significant rotational excitation does provide a possible explanation for some of the chlorine atom product flux seen at low E_T , at energies which would require the partner ClO fragment to carry $E_{INT} > D_0(\text{Cl—O})$. Moore *et al.*³² have calculated that the centrifugal barrier to dissociation of highly rotational excited ClO products could be as high as 30 kJ mol^{-1} , though, as Fig. 2 shows, even a barrier of this size is not sufficient to account for all of the slow Cl atoms in terms solely of channel (1). As shown below, the slowest Cl atoms arise from the three body dissociation (2).

Product vibration is the other contributor to the observed high levels of ClO internal excitation. Vibrational excitation of the ClO product is to be expected, simply on Franck–Condon grounds, given that the Cl—O equilibrium bond length in Cl₂O is longer than that of the ground state ClO radical by 0.126 \AA . We suggest that ClO product vibration is further enhanced by the nature of the 1B_2 excited state potential energy surface and, in what follows, we present a plausible explanation for the observed high levels of product vibrational excitation, the proposed involvement of the three body fragmentation process (2), and the strikingly different energy disposals in the product channels leading to ground (Cl) and spin-orbit excited (Cl*) atoms.

The rationale begins with a schematic potential energy surface for the excited 1B_2 state of Cl₂O, shown in the form of a contour plot, as a function of the two Cl—O bond lengths, in Fig. 8. For simplicity, we assume a constant bond angle similar to that of the ground state (110.9°)—an assumption supported by the foregoing analysis of the measured β parameter for forming Cl and Cl* products. The filled circle indicates the Franck–Condon region for excitation from the zero-point level of the ground state, while the shaded ellipse indicates the portion relevant for $\lambda_{\text{phot}} = 235 \text{ nm}$. Our positioning of the ellipse (which represents the starting point for trajectories or wave packet propagations representing the dissociation process of current interest) is guided by the knowledge that the $^1B_2 \leftarrow \tilde{X}^1A_1$ transition involves electron promotion to a Cl—O antibonding orbital and that the absorption maximum lies well to the red of the 235 nm photolysis wavelength. Clearly, trajectories starting from the ellipse on this model surface have sufficient energy to be able to sample all regions of configuration space involving extension of one or other or both of the Cl—O bonds. Thus we should expect a complete spectrum of energy disposals, ranging from Cl+ClO fragments with little vibrational energy (illustrated by trajectory A), through those with substantial product vibration (B), to the direct

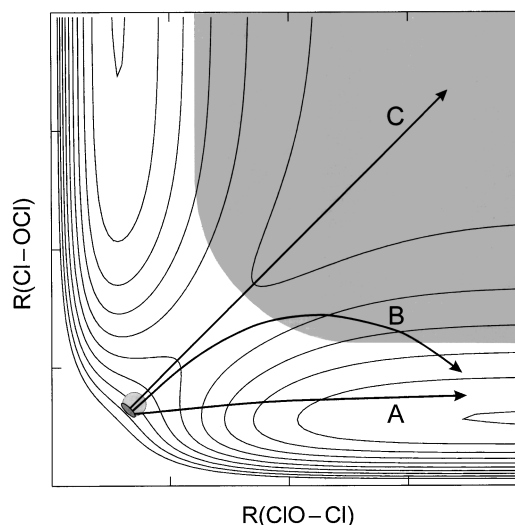


FIG. 8. Schematic potential energy surface for the dissociative 1B_2 excited state of Cl₂O. The filled circle represents the vertical Franck–Condon region starting from Cl₂O(\tilde{X}), $v=0$, while the ellipse indicates the portion relevant to excitation at 235 nm. Representative trajectories leading to Cl atoms, together with ClO(*X*) fragments with little (A) and extensive (B) vibrational excitation are shown, as is one leading to the three atomic products (C). It is assumed that there are many surface crossings or near crossings in the shaded region at long range which can mediate spin-orbit relaxation (see the text and Fig. 9).

(concerted) three body dissociations (C). In this picture, dissociation channel (2) is just a natural extension of channel (1), thus explaining the observation that all Cl (and Cl*) velocity subgroups show the same angular anisotropy. [Such would be unlikely if, as suggested previously,²⁸ any significant fraction of the observed Cl atom yield arose from secondary photolysis of the primary ClO(*X*) fragments.] The relative probabilities of branching into channels (1) and (2), and into the various ClO(*X*)_{*v*} product states associated with channel (1), will be determined by the detailed topology of the potential energy surface. We note that the present experiments suggest a much larger relative yield of slow Cl atoms arising from the three body dissociation (2) than do the earlier measurements at 248 nm.^{28,32} Such is consistent with the above picture in as much that the excess energy provided by a 248 nm photon is less, the ellipse representing the range of starting configurations will be less high up on the steeply repulsive wall, the dissociating trajectories will start with less momentum along the diagonal and be more prone to “veer off” into one of the Cl—OCl exit channels.

Finally, we turn to consider the observation that the energy disposal in the ClO fragment is sensitive to the spin-orbit state of the partner Cl atom: the $P(E_T)$ distributions in Figs. 2(a) and 2(b) show that internally “cold” ClO(*X*) fragments are formed exclusively with spin-orbit excited (Cl*) atoms. Cl atom spin-orbit selectivity has also been observed in the UV photodissociation of Cl₂CO,⁵² ClNO and CCl₄.⁵³ In these cases, as here, the spin-orbit selectivity is most readily explained in terms of one (or more) surface crossings in a selected area of configuration space. In the case of Cl₂O, the correlation diagram shown in Fig. 9 indicates that the 1B_2 excited state is actually the first excited state of Cl₂O

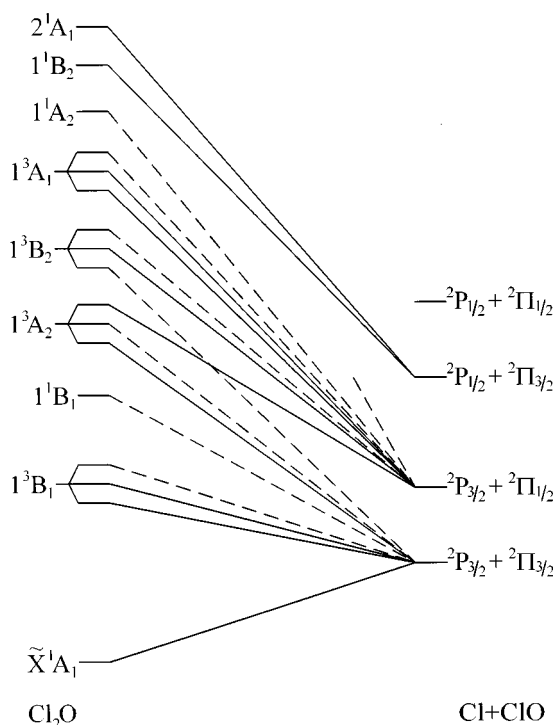


FIG. 9. Diagram showing the parent (Cl_2O)–product ($\text{Cl}+\text{ClO}$) correlations for bent (C_s) geometries. The energetic ordering of the electronic states of Cl_2O is taken from Ref. 21. For clarity of display, the parent and product sides of the diagram are plotted on different energy scales. States of a' and a'' symmetry (in C_s) are joined by solid and dashed lines, respectively.

that correlates diabatically with the spin-orbit excited Cl^* atom. The energetic ordering of the electronic states of the Cl_2O parent shown in this figure follows the *ab initio* results of Nickolaissen *et al.*,²¹ though our conclusion regarding the diabatic correlation between the 1^1B_2 excited state and spin-orbit excited Cl^* atoms is insensitive to any reordering of the lower lying, closely spaced 3A_2 , 3B_2 and 3A_1 states, or to the relative energetic ordering of the 1^1B_2 state and the 1A_2 state with which it is calculated to be in near resonance.

Thus we see that the asymptotic products of the model potential energy surface considered in Fig. 8 should in fact be $\text{Cl}^*+\text{ClO}(X)$, and that ground state Cl atom products (which we observe to dominate in the 235 nm photodissociation of Cl_2O) must arise as a result of radiationless transfer from the 1^1B_2 surface to one or more of the myriad of lower lying surfaces indicated in the correlation diagram (Fig. 9). Note that there will be many such surfaces: the various combinations of the ground state atoms [$\text{O}(^3P_J)+2\text{Cl}(^2P_J)$] correlate with no fewer than 27 singlet states of Cl_2O , plus 54 triplets and a further 27 quintet states. The model trajectories sketched in Fig. 8 even allow us to speculate on the region(s) of configuration space where this transfer occurs. The shaded area at larger $\text{Cl}-\text{O}$ bond lengths in Fig. 8 shows a plausible region of many surface intersections, which is consistent with experimental observations. Trajectories such as A, involving only one elongated bond are unaffected, and evolve to spin-orbit excited Cl^* atoms and ClO partners carrying little vibrational excitation, as before. How-

ever, the vast majority of trajectories (e.g., B and C) will pass into the region of crossings; if the nonadiabatic coupling is strong then most will cross to lower surface(s) and evolve to ground state Cl atoms and, given that all such trajectories involve some elongation of both $\text{Cl}-\text{O}$ bonds, vibrationally excited $\text{ClO}(X)$ fragments. Such a picture could also accommodate the observation of a larger Cl^*/Cl product branching ratio when Cl_2O is photolyzed at the longer wavelength of 248 nm⁴⁷ in as much that, again, in the language of Fig. 8, photoexcitation will place the starting configuration point for the trajectories nearer the saddle point, the subsequent momentum along the diagonal will be less and thus a larger fraction of the dissociating molecules may evolve along the exit valleys leading to Cl^*+ClO without encountering the region of the “seam.” Clearly, further studies of the wavelength dependence of the Cl^*/Cl branching ratio should prove fruitful as, too, would measurements of the quantum state population distributions in the $\text{ClO}(X)$ partner.

Photodissociation of HOCl at 235 and 266 nm

The measured anisotropy parameters for the Cl atoms resulting from 235 nm photolysis of HOCl ($\beta=1.7\pm 0.2$), and that deduced from analysis of the Doppler line shapes of the $\text{OH}(X)$ fragments resulting from photolysis at 266 nm ($\beta=1.3\pm 0.1$),⁴⁵ are both consistent with previous assignments^{10,11,14} of the intense UV absorption of HOCl centered at ~ 250 nm in terms of the $2^1A'-\tilde{X}^1A'$ transition arising as a result of electron promotion from an in-plane nonbonding p orbital on the Cl atom to a $\sigma_{\text{Cl}-\text{O}}^*$ antibonding orbital. The measured β values are less than the limiting value of +2. This could indicate that the transition moment is aligned some 18° off the axis of the breaking $\text{Cl}-\text{O}$ bond or may reflect an underlying contribution to the overall absorption cross section from the $1^1A''-\tilde{X}^1A'$ transition which is predicted to be more important at longer excitation wavelengths.^{10,11,14} Indeed, recent analyses of the Doppler line shapes of $\text{OH}(X)$ fragments resulting from the 355 nm photolysis of HOCl (which are best fit using an anisotropy parameter $\beta\sim -0.8$) confirm the involvement of this perpendicular transition at longer excitation wavelengths.⁴⁵ Alternatively, at least in the case of the Cl product measurements, the reduced β value may simply reflect an overlapping contribution from the less anisotropic recoil velocity distribution of the Cl atoms from Cl_2O photolysis (characterized by $\beta\sim 1.2$). The production of $\text{OH}(X)$ fragments exclusively in their ground vibrational state, and their modest rotational excitation, are both explicable in terms of Franck–Condon models and a potential energy surface for the $2^1A'$ state which is steeply repulsive along the $\text{Cl}-\text{O}$ stretching coordinate but fairly isotropic in the bending coordinate.^{7,8}

ACKNOWLEDGMENTS

M.N.R.A. is grateful to the EPSRC and NERC for financial support, in the form of equipment grants, a Senior Research Fellowship (M.N.R.A.), and a studentship (L.J.R.), to K. N. Rosser and Dr. B. J. Whitaker (University of Leeds) for their invaluable contributions toward the design and implementation of the Bristol ion imaging experiment, and to

Dr. A. J. Orr-Ewing for many helpful discussions. T.I. is grateful for a Hiroshima City University Grant for Special Academic Research (General Studies), M.K. is grateful to the Heiwa-Nakajima Foundation for support, while both M.N.R.A. and M.K. are grateful to the Japan Society for Promotion of Science, the British Council and the Royal Society for the Japan-UK Co-operative program which made this collaboration possible.

- ¹R. P. Wayne, *Chemistry of Atmospheres* (Clarendon, Oxford, 1994).
- ²R. P. Wayne, G. Poulet, P. Biggs, J. P. Burrows, R. A. Cox, P. J. Crutzen, G. D. Hayman, M. E. Jenkin, G. Le Bras, G. K. Moortgat, U. Platt, and R. N. Schindler, *Halogen Oxides: Radicals, Sources and Reservoirs in the Laboratory and in the Atmosphere* (European Commission, Luxembourg, Office for Official Publications of the European Communities, 1996), and references cited therein.
- ³M. J. Molina, T.-L. Tso, L. T. Molina, and F. C.-Y. Wang, *Science* **238**, 1253 (1987).
- ⁴L. T. Molina and M. J. Molina, *J. Phys. Chem.* **82**, 2410 (1978).
- ⁵E. A. Mishalanie, C. J. Rutkowski, R. S. Hutte, and J. W. Birks, *J. Phys. Chem.* **90**, 5578 (1986).
- ⁶R. Vogt and R. N. Schindler, *J. Photochem. Photobiol., A* **66**, 133 (1992).
- ⁷A. J. Bell, P. R. Pardon, C. G. Hickman, and J. G. Frey, *J. Chem. Soc., Faraday Trans.* **86**, 3831 (1990).
- ⁸C. G. Hickman, N. Shaw, M. J. Crawford, A. J. Bell, and J. G. Frey, *J. Chem. Soc., Faraday Trans.* **89**, 1623 (1993).
- ⁹A. J. Bell, S. A. Boggis, J. M. Dyke, J. G. Frey, R. Richter, N. Shaw, and M. Tabrizchi, *J. Chem. Soc., Faraday Trans.* **91**, 17 (1994).
- ¹⁰G. Hirsch, P. J. Bruna, S. D. Peyerimhoff, and R. J. Buenker, *Chem. Phys. Lett.* **52**, 442 (1977).
- ¹¹S. Nambu, K. Nakata, and S. Iwata, *Chem. Phys.* **135**, 75 (1992).
- ¹²S. Nambu and S. Iwata, *J. Phys. Chem.* **96**, 2103 (1992).
- ¹³H. Guo, *J. Phys. Chem.* **97**, 2602 (1993).
- ¹⁴A. R. Offer and G. G. Balint-Kurti, *J. Chem. Phys.* **101**, 10416 (1994); **104**, 563 (1996); *Chem. Phys. Lett.* **247**, 173 (1995).
- ¹⁵W. B. DeMore, S. P. Sander, D. M. Golden, R. F. Hampson, M. J. Kurylo, C. J. Howard, A. R. Ravishankara, C. E. Kolb, and M. J. Molina, *Chemical Kinetics and Photochemical Data for Use in Stratospheric Modelling, Evaluation No. 12*, JPL Publication 97-4 (1997).
- ¹⁶G. E. Herberich, R. H. Jackson, and D. J. Miller, *J. Chem. Soc. A* **1966**, 336.
- ¹⁷M. Nakata, M. Sugie, H. Takeo, C. Matsumara, T. Fukuyama, and K. Kuchitsu, *J. Mol. Spectrosc.* **86**, 241 (1981).
- ¹⁸C.-L. Lin, *J. Chem. Eng. Data* **21**, 411 (1976).
- ¹⁹H.-D. Knauth, H. Alberti, and H. Clausen, *J. Phys. Chem.* **83**, 1604 (1979).
- ²⁰J. B. Nee, *J. Quant. Spectrosc. Radiat. Transf.* **46**, 55 (1991).
- ²¹S. L. Nickolaisen, C. E. Miller, S. P. Sander, M. R. Hand, I. H. Williams, and J. S. Francisco, *J. Chem. Phys.* **104**, 2857 (1996).
- ²²F. Motte-Tollet, M.-P. Ska, G. M. Marston, I. C. Walker, M. R. F. Siggel, J. M. Gingell, L. Kaminski, K. Brown, and N. J. Mason, *Chem. Phys. Lett.* **275**, 298 (1997).
- ²³W. Finkelnburg, H. J. Schumacher, and G. Stieger, *Z. Phys. Chem. Abt. B* **15**, 127 (1931).
- ²⁴H. J. Schumacher and R. V. Townend, *Z. Phys. Chem. Abt. B* **20**, 375 (1933).
- ²⁵F. H. C. Edgecomb, R. G. W. Norrish, and B. A. Thrush, *Proc. R. Soc. London, Ser. A* **243**, 24 (1957).
- ²⁶N. Basco and S. K. Dogra, *Proc. R. Soc. London, Ser. A* **323**, 401 (1971).
- ²⁷S. P. Sander and R. R. Friedl, *J. Phys. Chem.* **93**, 4764 (1989).
- ²⁸C. M. Nelson, T. A. Moore, M. Okumura, and T. K. Minton, *J. Chem. Phys.* **100**, 8055 (1994).
- ²⁹S. Abramowitz and M. W. Chase, Jr., *Pure Appl. Chem.* **63**, 1449 (1991).
- ³⁰M. W. Chase, Jr., C. A. Davies, J. R. Downey, Jr., D. J. Frurip, R. A. McDonald, and A. N. Syverud, *J. Phys. Chem. Ref. Data* **14**, Suppl. 1 (1985).
- ³¹R. P. Thorn, Jr., L. J. Stief, S.-C. Kuo, and R. B. Klemm, *J. Phys. Chem.* **100**, 14,178 (1996), and references therein.
- ³²T. A. Moore, M. Okumura, and T. K. Minton, *J. Chem. Phys.* **107**, 3237 (1997).
- ³³D. W. Chandler and P. L. Houston, *J. Chem. Phys.* **87**, 1445 (1987).
- ³⁴A. J. R. Heck and D. W. Chandler, *Annu. Rev. Phys. Chem.* **46**, 335 (1995).
- ³⁵S. Arepalli, N. Presser, D. Robie, and R. J. Gordon, *Chem. Phys. Lett.* **118**, 88 (1985).
- ³⁶V. Skorokhodov, Y. Sato, K. Suto, Y. Matsumi, and M. Kawasaki, *J. Phys. Chem.* **100**, 12,321 (1996).
- ³⁷L. J. Rogers, M. N. R. Ashfold, Y. Matsumi, M. Kawasaki, and B. J. Whitaker, *Chem. Phys. Lett.* **258**, 159 (1996).
- ³⁸R. Liyanage, Y. A. Yang, R. Gordon, and R. W. Field, *J. Chem. Phys.* **101**, 6811 (1995).
- ³⁹M. Roth, C. Maul, and K.-H. Gericke, *J. Chem. Phys.* **107**, 10582 (1997), and references therein.
- ⁴⁰G. H. Cady, *Inorg. Synth.* **5**, 156 (1957).
- ⁴¹M. J. Molina, T. Ishiwata, and L. J. Molina, *J. Phys. Chem.* **84**, 821 (1980).
- ⁴²Y. Sato, Y. Matsumi, M. Kawasaki, K. Tsukiyama, and R. Bersohn, *J. Phys. Chem.* **99**, 16,307 (1995).
- ⁴³L. J. Rogers, M. N. R. Ashfold, Y. Matsumi, M. Kawasaki, and B. J. Whitaker, *J. Chem. Soc., Faraday Trans.* **92**, 5181 (1996).
- ⁴⁴T. Budinger and G. T. Gullberg, *IEEE Trans. Nucl. Sci.* **21**, 2 (1974).
- ⁴⁵H. Fujiwara and T. Ishiwata, *J. Phys. Chem.* (in press).
- ⁴⁶P. W. McLoughlin, C. R. Park, and J. R. Wiesenfeld, *J. Mol. Spectrosc.* **162**, 307 (1993), and references therein.
- ⁴⁷A. J. Chichinin, *Chem. Phys. Lett.* **209**, 459 (1993).
- ⁴⁸R. N. Zare, *Angular Momentum* (Wiley, New York, 1988).
- ⁴⁹M. R. Wedlock, R. Jost, and T. R. Rizzo, *J. Chem. Phys.* **107**, 10344 (1997).
- ⁵⁰G. H. Dieke and D. R. Crosley, *J. Quant. Spectrosc. Radiat. Transf.* **2**, 97 (1962).
- ⁵¹S. R. Langhoff, unpublished results reported in Ref. 28.
- ⁵²C. Maul, T. Haas, K.-H. Gericke, and F. J. Comes, *J. Chem. Phys.* **102**, 3238 (1995).
- ⁵³M. Kawasaki, K. Suto, Y. Sato, and Y. Matsumi, *J. Phys. Chem.* **100**, 19853 (1996).